

The transverse momentum spectra have traditionally been fitted by blast-wave fits [14] to extract kinetic freeze-out temperature and radial flow velocity [15–19]. But the blast-wave model cannot be used to describe the spectra for higher p_T values. Recent studies of the thermodynamical parameters in relativistic collisions in the Tsallis framework shows a satisfactory fitting of the full p_T spectrum in both pp as well as in heavy-ion collisions [4, 20]. A formalism of the thermodynamically consistent form of the Tsallis distribution and the measurement of temperature in pp system is given in Ref. [3]. The Tsallis distribution provides an excellent description of p_T spectra to a large p_T range in pp collisions at LHC energies Ref. [5, 20]. The thermodynamical properties in pp collisions at the LHC energies using the different forms of the Tsallis distribution can be found in Ref. [6–9]. Dependence of Tsallis parameters on the particle multiplicity, p_T ranges in pp system are reported in Ref. [21]. In heavy-ion collisions, the freeze-out properties, such as temperature, energy density, pressure, and entropy have been studied in Ref. [4]. The nuclear modification factor using the Tsallis statistics has been studied in Ref. [10, 12], whereas the fluctuations in thermodynamic parameters are reported in Ref. [11].

In this work, we present the results of thermodynamic freeze-out parameters from the fits of transverse momentum (p_T) spectra of charged pions as well as all charged particles using non-extensive Tsallis fitting function in heavy-ion collisions corresponding to eight different collision energies at RHIC and two collision energies at the LHC. The dependencies of the parameters on the collision centrality, collision energy and fitting ranges in p_T are investigated. In section 2, we discuss the formulation of the Tsallis distribution and methodology of fitting the p_T spectra. In section 3, we present Tsallis fittings of the p_T spectra at different centrality, energy and p_T ranges. In section 4, present the Tsallis fit parameters and discuss their relevances for different collision energies. A discussion on the results is given in section 5. Finally, the paper is summarized in section 6.

2 Tsallis statistics and methodology

The non-extensive Tsallis form of the Boltzmann-Gibbs distribution in terms of energy (E), temperature (T), and chemical potential (μ) of a system can be expressed as [1, 2],

$$f(E, q, T, \mu) \equiv \exp_q \left(-\frac{E - \mu}{T} \right) \equiv \left(1 + (q - 1) \frac{E - \mu}{T} \right)^{-\frac{1}{q-1}} \quad (1)$$

The $\exp_q(x)$ has the form,

$$\exp_q(x) \equiv \begin{cases} (1 + (q - 1)x)^{\frac{1}{q-1}} & \text{if } x > 0, \\ (1 + (1 - q)x)^{\frac{1}{1-q}} & \text{if } x \leq 0, \end{cases} \quad (2)$$

where q is the entropy index which measures the degree of non-additivity of the entropy or deviation from the equilibrium of the system. In general, $q \geq 1$. In equilibrium case, *i.e.*, in the limit $q \rightarrow 1$, $\exp_q(x) \rightarrow \exp(x)$. Therefore, Eq. 1 is simplified to the extensive Boltzmann-Gibbs form,

$$f_{q \rightarrow 1}(E, q, T, \mu) \equiv f_{BG}(E, T, \mu) \equiv \exp \left(-\frac{E - \mu}{T} \right). \quad (3)$$

The Tsallis form with thermodynamical consideration of the invariant momentum distribution of the particles has been introduced and discussed in [3, 22]. The relevant thermodynamic quantities, such as, particle number density (n), entropy (s), energy density (ϵ), and pressure (P) have been formulated using the Tsallis function (Eq. 1) as,

$$n = g \int \frac{d^3p}{(2\pi)^3} f^q, \quad (4)$$

$$s = -g \int \frac{d^3p}{(2\pi)^3} \left(\frac{f - f^q}{1 - q} - f \right), \quad (5)$$

$$\epsilon = g \int \frac{d^3p}{(2\pi)^3} E f^q, \quad (6)$$

$$P = g \int \frac{d^3p}{(2\pi)^3} \frac{p^2}{3E} f^q. \quad (7)$$

The expression of the invariant momentum distribution can be obtained from the particle number density as given in Eq. 4 as,

$$E \frac{d^3N}{dp^3} = \frac{gV}{(2\pi)^3} E \left(1 + (q - 1) \frac{E - \mu}{T} \right)^{-\frac{q}{q-1}}. \quad (8)$$

Here N is the particle number, and V is referred as the volume of the system which depends on the q . Therefore, V is not necessarily the volume of the system, but serves as a normalization factor of the Tsallis distribution. For non vanishing chemical potential, Eq. 8 can be rewritten in terms of transverse mass (m_T) and rapidity (y) in the form,

$$\frac{1}{2\pi p_T} \frac{d^2N}{dp_T dy} = \frac{gV}{(2\pi)^3} m_T \cosh(y) \left(1 + (q - 1) \frac{m_T \cosh(y) - \mu}{T} \right)^{-\frac{q}{q-1}}. \quad (9)$$

The invariant yields, $\frac{1}{2\pi p_T} \frac{d^2 N}{dp_T dy}$ is an experimentally measured observable. Therefore, the Tsallis parameters q , T can be obtained from experimentally measured invariant momentum distributions using the fitting function as given in Eq. 9, with μ as an input.

In literature, more than one version of Tsallis distribution can be found to interpret the data of the pp collisions [7, 9, 13, 23] and $A-A$ system [6–9]. A comparative study of the success of different versions of Tsallis distribution are reported in [9, 13]. The Tsallis form with thermodynamical description can explain the pp collisions system well [3, 21, 22, 24–26] even for p_T range up to 200 GeV/c [20]. The thermodynamically derived Tsallis distribution also successfully describe $A-A$ collision system as found in recent studies [4, 10].

A different kind of Tsallis distribution is used by the STAR [27], PHENIX [28, 29], ATLAS [30], CMS [31] and ALICE [32–35] collaborations as in the expression below,

$$\frac{1}{2\pi p_T} \frac{d^2 N}{dp_T dy} = \frac{1}{2\pi} \frac{dN}{dy} \frac{(n-1)(n-2)}{nC(nC+m(n-2))} \left(1 + \frac{m_T - m}{nC}\right)^{\frac{1}{q-1}}, \quad (10)$$

where n , C are the fitting parameters and m is the rest mass of the particle. At mid-rapidity and zero chemical potential Eq. 10 has same dependency on transverse momentum as in Eq. 9 except the additional m_T dependency. The incorporation of m_T in Eq. 9 has more consistent behavior of q and T whereas no clear pattern of n and C can be found [3]. In this present study, Tsallis distribution of thermodynamical consistent form given in Eq. 9 has been used.

The Tsallis form of the transverse momentum distribution for all charged particles is a sum of Tsallis distributions of the most dominating particles namely π^\pm , K^\pm , protons and anti-protons. In this case, the conversion from rapidity to pseudo-rapidity phase-space is made using a Jacobian ($J(y, \eta)$) of the form,

$$\frac{dN}{dp_T d\eta} = \sqrt{1 - \frac{m^2}{m_T^2 \cosh^2(y)}} \frac{dN}{dy dp_T}. \quad (11)$$

At mid-rapidity ($y \approx 0$), this can be simplified as

$$\frac{dN}{dp_T d\eta} = \frac{p_T}{m_T} \frac{dN}{dy dp_T}. \quad (12)$$

The expression of the Tsallis distribution for all charged particle pseudo-rapidity distribution at mid rapidity can be given as,

$$\frac{d^2 N_{\text{ch}}}{dp_T d\eta} = 2p_T^2 \frac{V}{(2\pi)^2} \sum_{i=1}^3 g_i \left(1 + (q-1) \frac{m_{T,i} - \mu}{T}\right)^{-\frac{q}{q-1}}.$$

$$(13)$$

Here the sum runs for three kind of the particles π^+ , K^+ , and p . The factor 2 in front of the right side takes into account of the associated anti-particles, π^- , K^- , and \bar{p} . The degeneracy factors are unity for pions and kaons and 2 for protons. At mid-rapidity, Eq. 9 reduces to the form,

$$\frac{1}{2\pi p_T} \frac{d^2 N}{dp_T dy} = \frac{gV}{(2\pi)^3} m_T \left(1 + (q-1) \frac{m_T - \mu}{T}\right)^{-\frac{q}{q-1}}. \quad (14)$$

This equation (14) has been used to fit invariant momentum spectra of identified particles. The centrality dependent finite chemical potential μ has been considered for the RHIC energy [15, 36], whereas at LHC energies μ has been approximated to zero.

3-Fits of the p_T spectra

Detailed analysis of the transverse momentum spectra of produce particles provides important information regarding the particle production mechanisms. We have fitted the p_T spectra of pions and all charged particles in heavy-ion collisions at RHIC and LHC. At RHIC, the experimental data of Au-Au collisions from the beam energy scan (BES-I) program are available for $\sqrt{s_{NN}} = 7.7, 11.5, 14.5, 19.6, 27, 39$ GeV [15, 16] as well as at 62.4 and at the top energy of 200 GeV. Fine centrality binning data from PHENIX collaboration at $\sqrt{s_{NN}} = 200$ GeV [37] are also fitted. At the LHC, data published by the ALICE collaboration for p_T spectra of identified charged particles in Pb-Pb collisions at $\sqrt{s_{NN}} = 2.76$ TeV [18, 38] and at 5.02 TeV [19] have been included in our study. In addition, p_T spectra of all charged particles (N_{ch}) measured by ALICE at $\sqrt{s_{NN}} = 2.76$ and 5.02 TeV [39, 40] are also used. In Table 1, we summarize the experimental datasets along with the collision energy, colliding system, pseudo-rapidity (η) range, p_T range, and centrality binning in the percentage of the cross-section.

The fits to the transverse momentum spectra at all collision energies as given in Table 1 are performed by the expression of Tsallis distribution as in Eq. 14. The transverse momentum spectra with Tsallis fitting of positively charged pions (π^+) at different centrality bins in Au-Au collisions at $\sqrt{s_{NN}} = 7.7$ GeV to 39 GeV measured by the STAR collaboration from the RHIC BES-I [15, 16] program are shown in Fig. 1. The data are available for p_T range up to 2 GeV/c, and so the fits, represented by the solid lines, are also made up to this p_T range. The Tsallis distribution provides very

Table 1 Collision energy, collision species, observed particles, centrality binning, pseudo-rapidity, and transverse momentum range of p_T spectra from the STAR, PHENIX and ALICE experiments.

$\sqrt{s_{NN}}$ (GeV)	Collision system	Particles	$ \eta $	p_T range (GeV)	Centrality (%)	Experiment
7.7, 11.5, 19.6, 27, 39	Au-Au	π^+, π^-	0.1	0.25-2.0	0-5, 5-10, 10-20, 20-30, 30-40, 40-50, 50-60, 60-70, 70-80	STAR [15]
14.5	Au-Au	π^+, π^-	0.1	0.2-2.0	0-5, 5-10, 10-20, 20-30, 30-40, 40-50, 50-60, 60-70, 70-80	STAR [16]
62.4	Au-Au	π^+, π^-	0.5	0.2-10	0-10, 10-20, 20-40, 40-80	STAR [41]
200	Au-Au	π^+, π^-	0.5	0.3-12	0-12, 10-20, 20-40, 40-60, 60-80	STAR [42]
200	Au-Au	π^+, π^-	0.26	0.2-3	0-5, 5-10, 10-15, 15-20, 20-30, 30-40, 40-50, 50-60, 60-70, 70-80, 80-92	PHENIX [37]
2760	Pb-Pb	π^+, π^-	0.5	0.1-3	0-5, 5-10, 10-20, 20-30, 30-40, 40-50, 50-60, 60-70, 70-80, 80-90	ALICE [18]
2760	Pb-Pb	$\pi^+ + \pi^-$	0.5	0.1-20	0-5, 5-10, 10-20, 20-30, 30-40, 20-40, 40-50, 40-60, 60-80	ALICE [38]
2760	Pb-Pb	N_{ch}	0.8	0.15-50	0-5, 5-10, 10-20, 20-30, 30-40, 40-50, 50-60, 60-70, 70-80	ALICE [39]
5020	Pb-Pb	$\pi^+ + \pi^-$	0.5	0.1-20	0-5, 5-10, 10-20, 20-30, 30-40, 40-50, 50-60, 60-70, 70-80, 80-90	ALICE [19]
5020	Pb-Pb	N_{ch}	0.8	0.15-50	0-5, 5-10, 10-20, 20-30, 30-40, 40-50, 50-60, 60-70, 70-80	ALICE [40]

good fits of the data at all centralities, which is evident from the ratio of the experimental data to the fit value as shown in the lower panel of the figure. The fits of the p_T spectra of π^- distributions have turned out to be of similar quality as of the π^+ distributions.

Fig. 2 shows the p_T spectra along with the corresponding Tsallis fits for Au-Au collisions at $\sqrt{s_{NN}} = 62.4$ and 200 GeV from STAR [41, 42] experiment with the available p_T ranges up to 10 GeV/c and 12 GeV/c, respectively. The left panels of the figure show the fits of the p_T range up to 2 GeV/c and the right panels provide the Tsallis fitting of the entire p_T spectrum. The ratios of the data to fit values are shown in the lower part of the figures. We see that the Tsallis distribution fits the spectra well in all cases, even up to mid- p_T ranges. But the fit parameters turn out to be dependent on the fit ranges in p_T . The results of the fits are discussed in detail in the next section.

In Fig. 3, we present the transverse momentum spectra of all charged pions ($\pi^+ + \pi^-$) for different centrality bins for Pb-Pb collisions at $\sqrt{s_{NN}} = 2.76$ TeV from the ALICE [38] collaboration. The fits with the Tsallis distribution function have been shown for three different p_T ranges, where the left, middle, and the right panels in the figure correspond to p_T ranges up to 2 GeV/c, 10 GeV/c and 20 GeV/c, respectively. The lower part of the figures give the ratio of the data to the fitted values. These ratios show that the fitting is in very good agreement with the data for peripheral events, whereas

some deviations have been observed for central collisions and at large p_T . Furthermore, it is observed that the fit parameters vary according to the fitting ranges in p_T .

4 Results of the Tsallis fit parameters

In this section, we present the results of the fitting of p_T distributions as a function of collision centrality, collision energy as well as the fit range in p_T . The results are presented for the Tsallis parameters, q , T , and the normalization volume, V .

4.1 Centrality dependence of Tsallis parameters

In the previous section, we have presented p_T distributions for different collision energies and collision centralities. The collision centralities have been shown in terms of percentage of cross section. For a given centrality window, the centrality can also be expressed in terms of average number of participating nucleons (N_{part}). As the centrality bins in the data as shown in Table 1 are different, it is useful to express the centrality in terms of N_{part} . In Fig. 4, we present the variation of q , T , and V as a function of N_{part} for positively charged pions at RHIC energies, and for all charged pions at LHC energies. The parameters obtained from π^+ and π^- spectra of ALICE data [18] are similar to the results from all

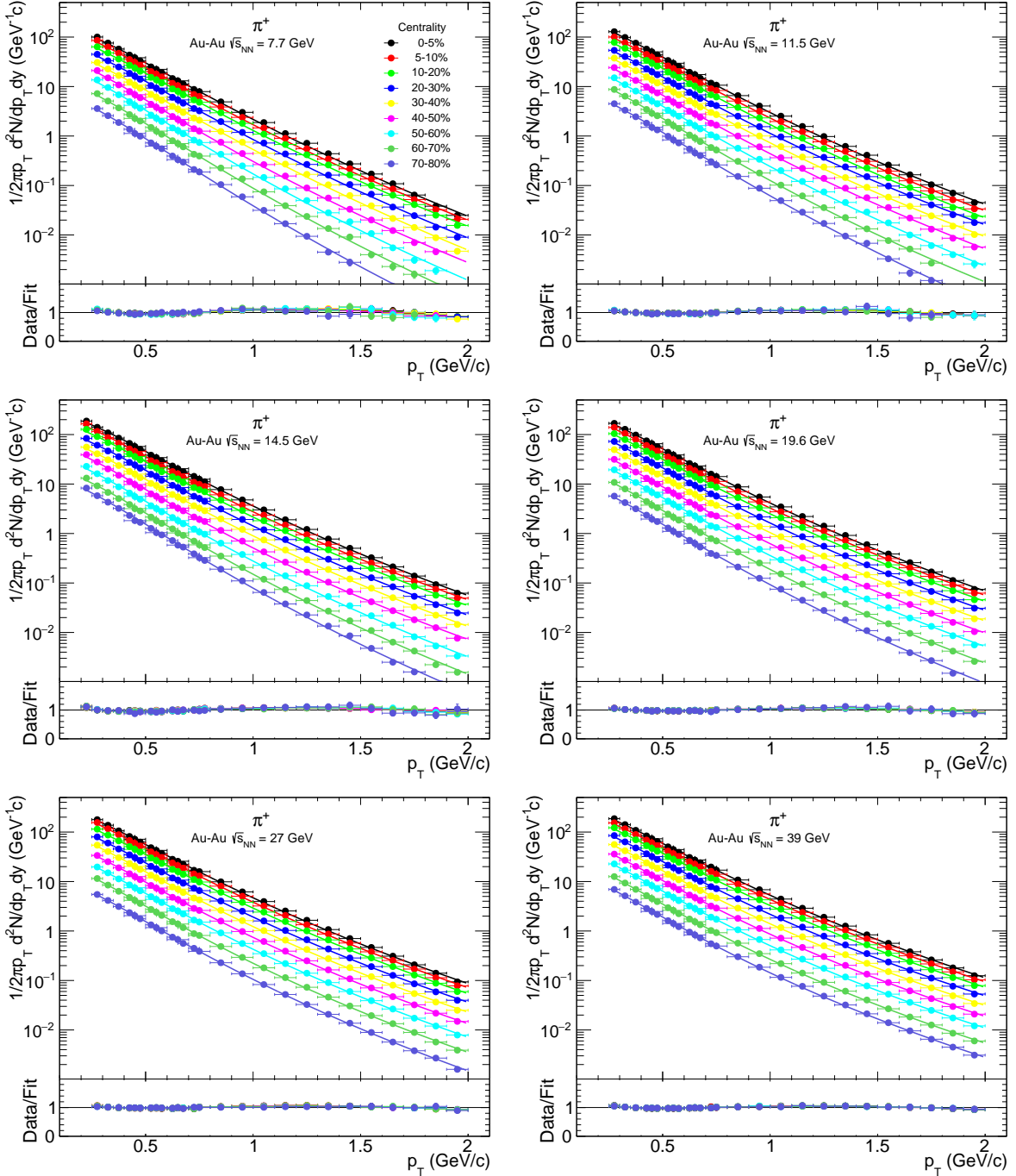


Fig. 1 Transverse momentum distributions of π^+ for different centralities at $\sqrt{s_{NN}} = 7.7, 11.5, 14.5, 19.6, 27, 39$ GeV, measured by the STAR experiment [15, 16]. The solid lines represent fitting by the Tsallis distribution as given in Eq. 14. The lower parts of the figures represent the ratios of the data to that of the fitting values.

charged pions (not shown here). All the fits are made for maximum values of p_T up to 2 GeV/c. The following observations are made regarding the centrality and collision energy dependence of these parameters:

- The Tsallis parameter, q , systematically increases from low to high collision energies. For collision energies below $\sqrt{s_{NN}} = 27$ GeV, q increases from most

peripheral collisions to up to a value of $N_{\text{part}} \approx 80$ ($\approx 50\%$ centrality), and then remains constant. For $\sqrt{s_{NN}} = 27$ GeV, q remains constant as a function of centrality, and beyond this energy, the values of q decreases in going from peripheral to central collisions. Thus, the nature of q as a function of centrality changes around $\sqrt{s_{NN}} = 27$ GeV.

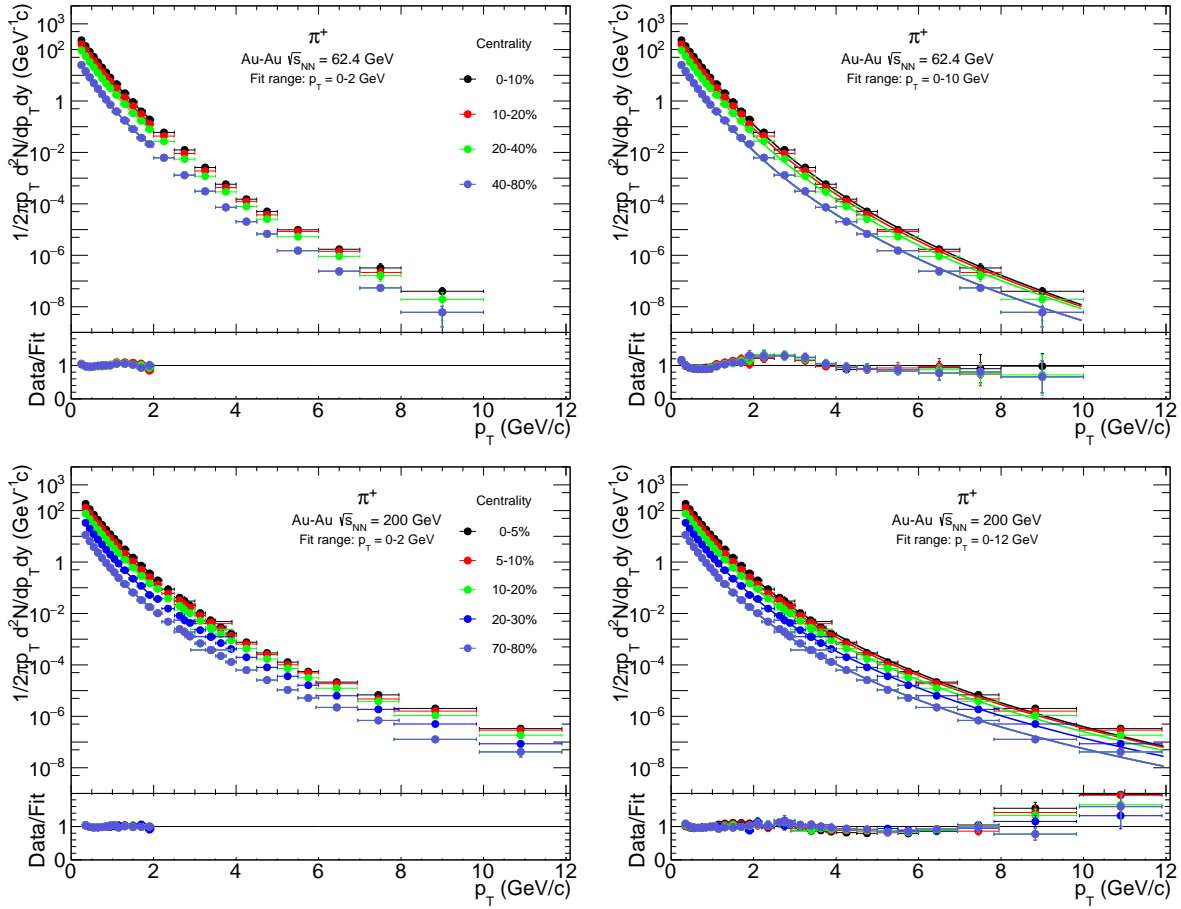


Fig. 2 Transverse momentum distributions of π^+ for different centralities at $\sqrt{s_{NN}} = 62.4$ and 200 GeV measured by the STAR experiment [41, 42]. The left and right panels correspond to fitting ranges of p_T up to 2 GeV/c and up to the full p_T range, respectively. The solid lines represent fitting by the Tsallis distribution as given in Eq. 14. The lower parts of the figures represent the ratios of the data to that of the fitting values.

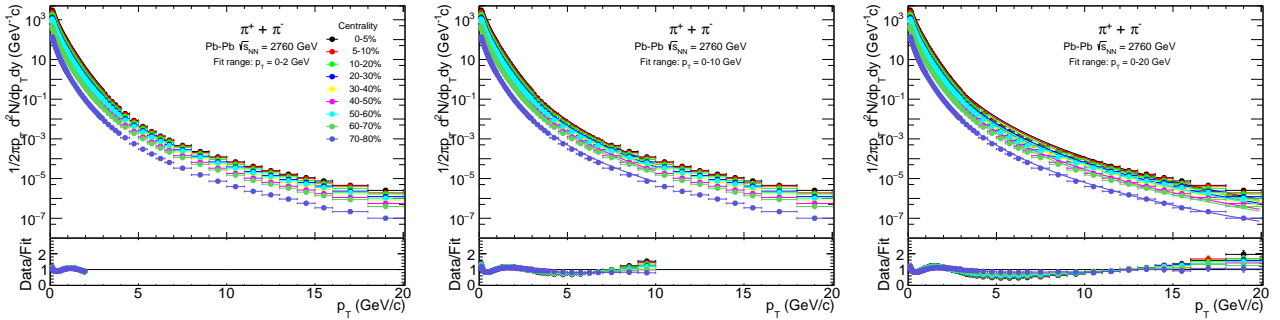


Fig. 3 Transverse momentum distribution of $\pi^+ + \pi^-$ for different centralities at $\sqrt{s_{NN}} = 2.76$ TeV measured by the ALICE experiment [38]. The left, middle and right panels correspond to fitting ranges of p_T up to 2 GeV/c, 10 GeV/c and 20 GeV/c, respectively. The solid lines represent fitting by the Tsallis distribution as given in Eq. 14. The lower parts of the figures represent the ratios of the data to that of the fitting values.

- The Tsallis temperature, T , decreases from low to high collision energies. For all collision energies, the values of T increase from peripheral to central collisions.
- The normalization parameter, V , increases from low to high collision energies. For all collision energies, V

increases monotonically from peripheral to central collisions.

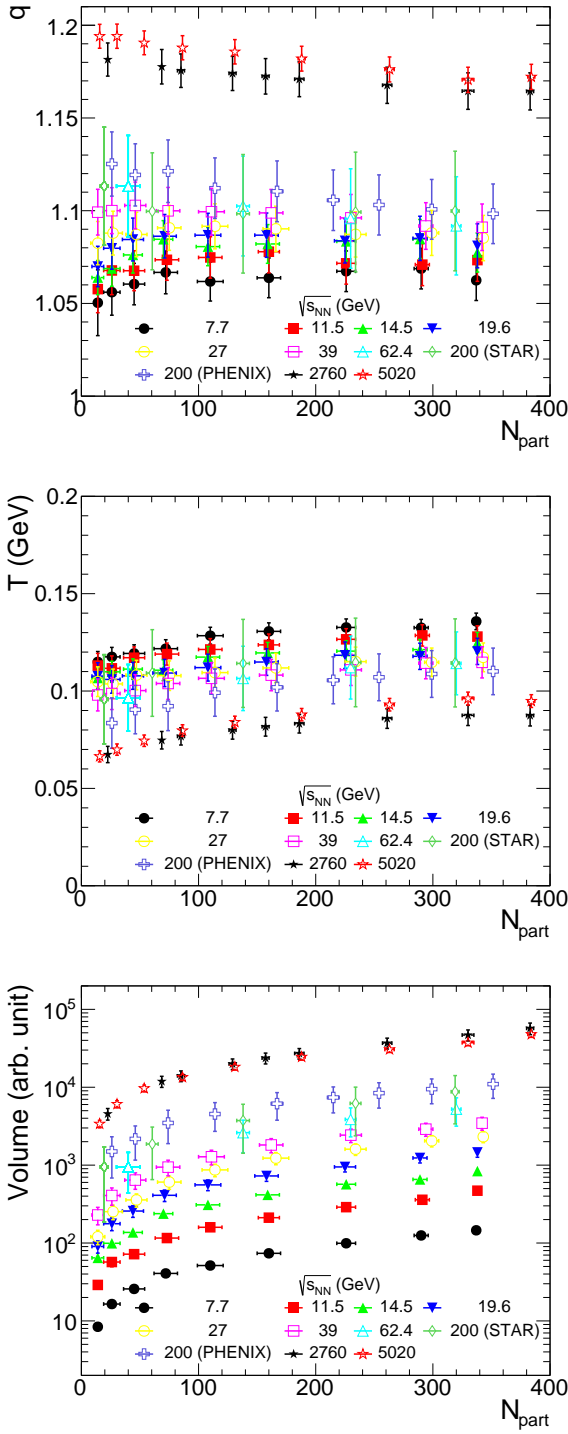


Fig. 4 Tsallis parameters, q , T , and the normalization factor, V as a function of number of participants, N_{part} , obtained by fitting the p_T spectra up to 2 GeV/c for π^+ at RHIC energies from STAR [15, 16, 41, 42], and PHENIX [37], and all charged pions at LHC energies from ALICE [19, 38].

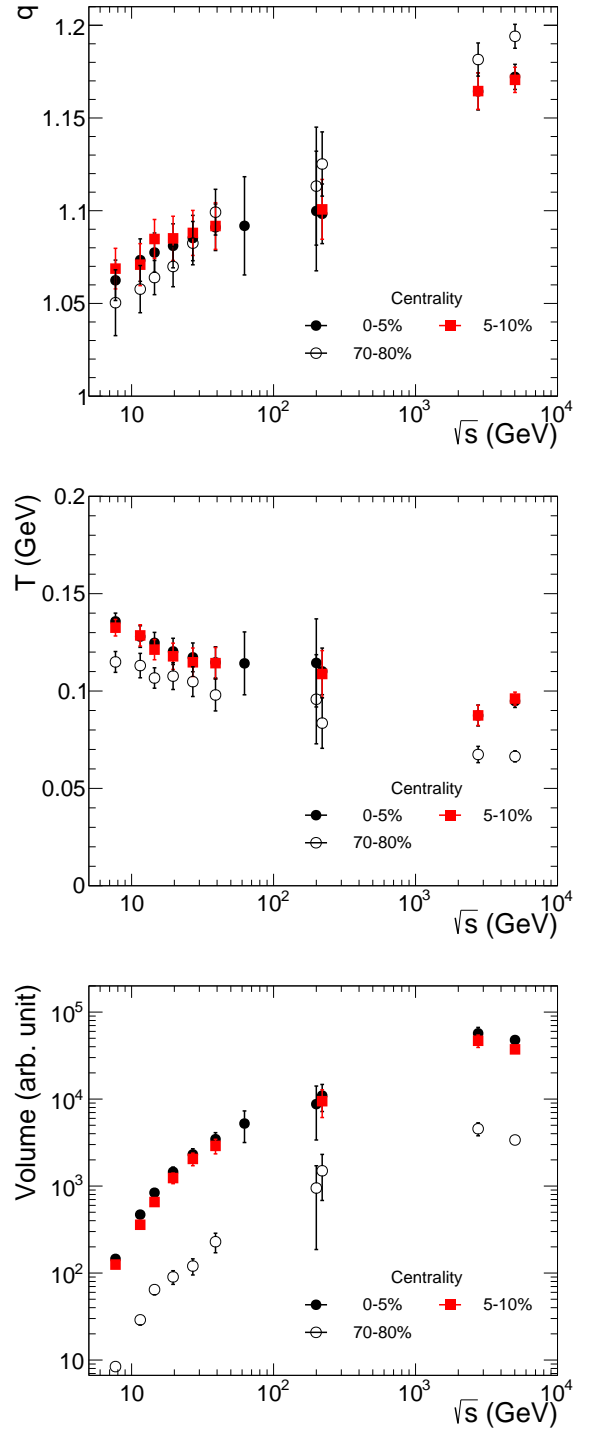


Fig. 5 Tsallis parameter q , T , and the normalization factor, V as a function of collisions energy, $\sqrt{s_{\text{NN}}}$, for three different centralities obtained by fitting the p_T spectra up to 2 GeV/c for π^+ at RHIC energies from STAR [15, 16, 41, 42], and PHENIX [37], and all charged pions at LHC energies from ALICE [19, 38]. PHENIX results are shifted to right for clarity.

4.2 Collision energy dependence of Tsallis parameters

The variations of the Tsallis parameters, q , T , and the normalization parameter, V , are scanned over the collision energy $\sqrt{s_{NN}}$ from RHIC to LHC energies. The results of the fits to p_T spectra up to a value of 2 GeV/ c are presented in Fig. 5. At RHIC energies, the fits are performed for π^+ , and at the LHC energies, the fits are presented for $\pi^+ + \pi^-$. For clarity, results are presented for only central (0-5%, 5-10%) and peripheral (70-80%) collisions. The following observations are made regarding the collision energy dependence of these parameters:

- The parameter q as a function of collisions energy shows that for all centralities q increases with the increase of collision energy. A closer look at the centrality dependence shows that at low collision energy (below $\sqrt{s_{NN}} = 27$ GeV), q increases from peripheral to central collisions, whereas at higher energies, the q decreases from peripheral to central collisions.
- The parameter T decreases with the increase of the collision energy. Another important observation is that T increases from peripheral to central collisions at all collision energies.
- The variation of V with collisions energy shows that, V increases consistently with increasing $\sqrt{s_{NN}}$. This is reasonable as the system size and hence particle productions increases with $\sqrt{s_{NN}}$ and centrality.

4.3 Behavior of Tsallis parameters for different p_T ranges

The Tsallis function is successful in fitting p_T distributions over a broad range. The fit parameters have a strong dependence on the selection of the fitting range in p_T . Fig. 6 shows the variation of the Tsallis fit parameters, q , and T as a function of N_{part} on the p_T range for Pb-Pb collisions at 2.76 TeV. The results correspond to the fits of p_T spectra of $\pi^+ + \pi^-$ and for the all charged particles (N_{ch}) at $\sqrt{s_{NN}} = 2.76$ TeV [38,39]. The p_T ranges are labeled in the figure with a closed and open markers correspond to the $\pi^+ + \pi^-$ and N_{ch} , respectively. We observe that:

- for all centralities, q values are distinctly different for p_T range up to 2 GeV/ c , whereas for ranges of 5, 7, 10 GeV/ c the values are almost same. In most of the cases, q decreases from peripheral to central collisions.
- the temperature increases from peripheral to central collisions for all p_T ranges. T is found lower for N_{ch} compared to $\pi^+ + \pi^-$ for all the p_T ranges. The values of T are lower for p_T range up to 2 GeV/ c ,

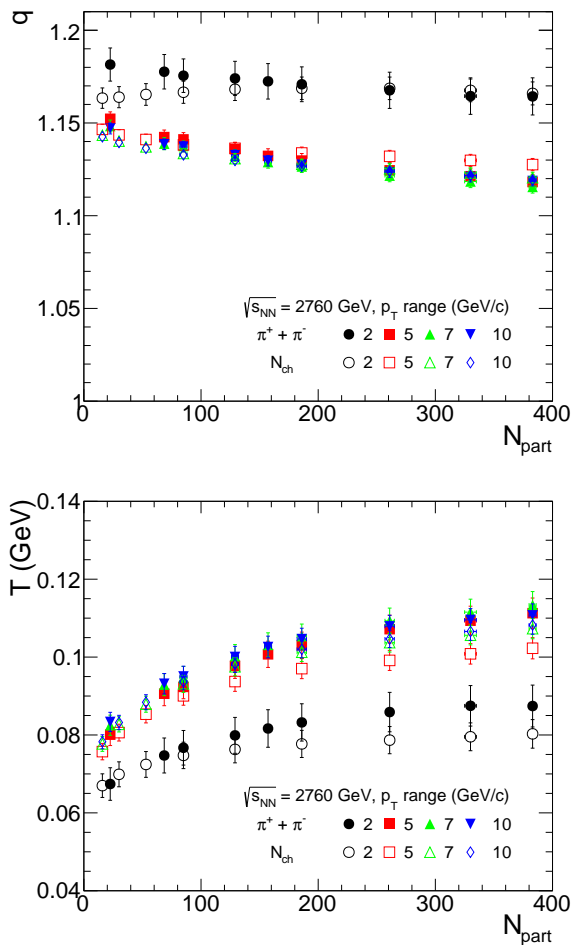


Fig. 6 Tsallis parameters q , T as a function of centrality (N_{part}) for different p_T ranges at $\sqrt{s_{NN}} = 2760$ GeV [38,39]. The closed and open markers correspond to the parameters of the all charged particles (N_{ch}) and charged pions ($\pi^+ + \pi^-$), respectively.

whereas for ranges of 5, 7, 10 GeV/ c the values are very close to each other.

The behavior of the fit parameters have been explored further by plotting these as a function of the p_T ranges for different collision energies. Depending on the availability of the experimental data, the p_T ranges have been selected up to 2, 3, 5, 7, 10, 12, 15, 20, and 50 GeV/ c . The evolution of the Tsallis parameters with p_T range selections are shown in Fig. 7. The results shown in the figure correspond to the fit values of all possible p_T spectra at $\sqrt{s_{NN}} = 62.4, 200, 2760$ and 5020 GeV of all charged particles, $\pi^+ + \pi^-$, and π^+ . The closed and open markers correspond to the most central (0-10%) and peripheral collisions (70-80%), respectively. We observe that,

- for central collisions, q decreases with p_T , attains a minimum at around 5-10 GeV/ c , and then slowly in-

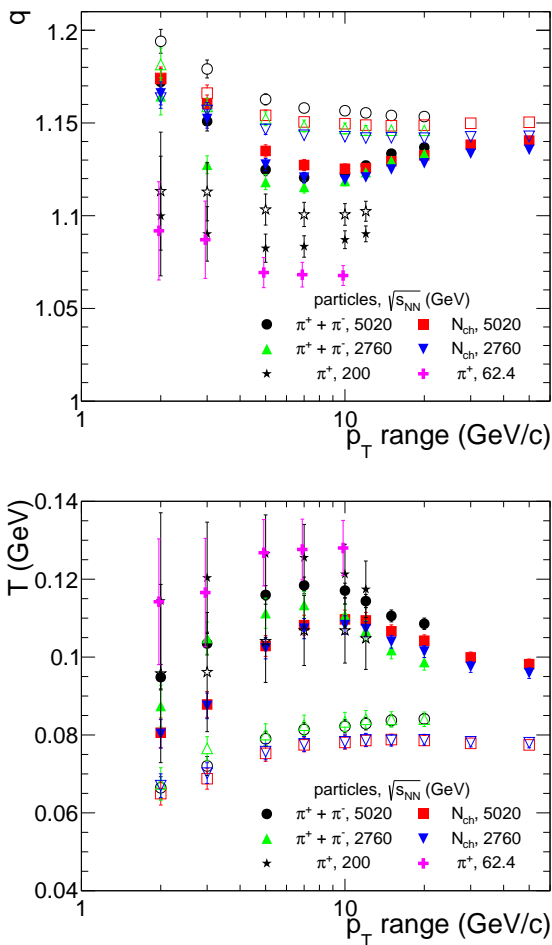


Fig. 7 Tsallis parameters q , T as a function of p_T range for different collision energies. The parameters are at $\sqrt{s_{NN}} = 62.4, 200, 2760, 5020$ GeV for all charged particles N_{ch} , all charged pions ($\pi^+ + \pi^-$) and π^+ as labeled by different markers [19, 38–42]. The closed and open markers correspond to the parameters of the central and peripheral collisions.

creases. However, in peripheral collisions, q initially decreases with p_T and then remains constant at p_T afterwards.

- for central collisions, T increases with p_T , attain a maximum at p_T around 5–10 GeV/c, and then it decreases slowly. However, for the peripheral collisions, T increases slowly and then it becomes constant.
- p_T range dependency of the Tsallis parameters are clearly observed for central collisions. However, for the peripheral collisions, both the parameters, q , T , remain unchanged at mid- p_T regions. From this observation, we may infer that different physics processes, such as, thermal, coalescence, contribution from jets, etc., dominate in particle production mechanism depending on the p_T domain and collision centrality at a given $\sqrt{s_{NN}}$.

5 Discussion

From the above section, we observe that the Tsallis parameters vary with respect to the fitting range in p_T , centrality of the collision and collision energy. Can these variations in q , and T be compared to the results of the blast-wave fits to the p_T spectra? The blast-wave fits to available experimental have been reported by the STAR and ALICE experiments [15, 16, 18, 19]. It is observed that with the increase of collision energy beyond $\sqrt{s_{NN}} = 7.7$ GeV, the kinetic freeze-out temperature (T_{kin}) decreases whereas radial flow velocity (β) increases [15]. The behavior of T_{kin} and β for central collisions as a function of collision energy is similar to the Tsallis fit parameters, T and q . As a function of centrality, T_{kin} decreases from peripheral to central collisions in blast-wave fits. Whereas temperature increases with centrality in the Tsallis fits, this is different from the observation from the blast-wave, as has been seen earlier [4].

The correlation between the Tsallis fit parameters can be better understood by making profile plots of q and T as shown in Fig. 8. In the upper panel of Fig 8, q vs. T is plotted for fits up to p_T of 2 GeV/c for pions in case of all collision energies and collision centralities. For collision energies above 27 GeV, the variation of q and T follow a linear pattern for all centralities, where central collisions have high T and low q and peripheral collisions have lower T and higher q . However, below 27 GeV, an interesting pattern is observed. A reversal in the behavior of q vs. T is observed from peripheral to central collisions. With the increase of centrality from peripheral collisions, the value of T first increases with q and from mid-central collisions there is an increase in T with no significant change in q . This trend has not been observed for freeze-out parameters obtained in the case of blast-wave fits.

In the lower panel of Fig 8, we plot the variation of q and T for fit ranges up to p_T of 10 GeV/c for collision energies at 62.4 GeV and above. Here the pattern is similar to what is observed for higher energy collisions when fitted up to p_T of 2 GeV/c, although the values of q and T are different for same collision energies. At the LHC energies, fit values from charged particles and identified charged pions are plotted. For the same values of q , the extracted T are larger for $\pi^+ + \pi^-$ compared to charged particles.

6 Summary

In high-energy collisions, the transverse momentum spectra of produced particles provide crucial information regarding the particle production mechanisms as well as

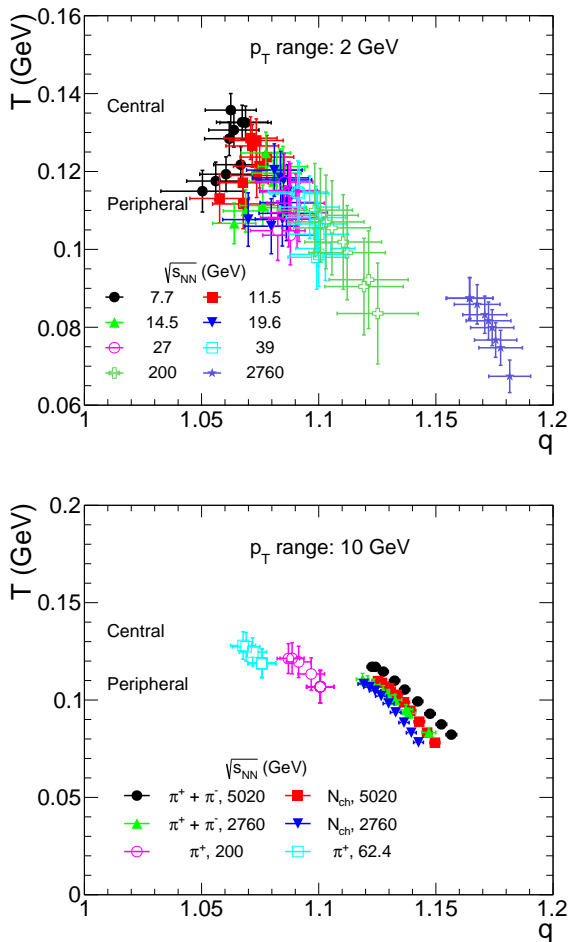


Fig. 8 Variation of Tsallis temperature (T) with q for different centrality classes and collision energies for all charged particles within (left panel) $p_T < 2$ GeV/ $c.$, and (right panel) $p_T < 10$ GeV/ $c.$

thermodynamic properties of the system at freeze-out. We have analyzed the p_T spectra of charged particles and identified pions produced in Au–Au collisions at eight energies at RHIC and Pb–Pb collisions at two energies at LHC using a function corresponding to non-extensive Tsallis statistics. The Tsallis function fits all the spectra very well for a wide range in p_T , with fit parameters, q , which is the entropy index measuring the degree of non-additivity of the entropy of the system, temperature, T , and a normalization parameter V which is proportional to the volume of the system.

For each centrality and collision energy, we have extracted q , and T . With the increase of collision energy, q systematically increases and T decreases. The centrality dependence of q turns out to be dependent on the collision energy. For collision energies below $\sqrt{s_{NN}} = 27$ GeV, q increases from most peripheral collisions to up to a value of $N_{part} \geq 80$ beyond which it remains constant.

At higher collision energies, q decreases from peripheral to central collisions. The values of T increase from peripheral to central collisions. The parameter, V , increases monotonically with centrality and collision energy. A dependence of the parameters, q, T , on the fitting range in p_T has been observed, which also depends on the collision energy. This has been understood as different physics processes dominate different p_T domains.

The p_T spectra have been previously fitted by blast-wave model for low p_T range, which yields kinetic freeze-out temperature and radial flow velocity, β . These parameters show a two-dimensional anti-correlation band, *i.e.*, higher values of kinetic temperature correspond to lower values of β . Both the parameters show rapid increase at very low collision energies. After this, temperature decreases with collision energy whereas β has a steady increase. To compare the blast wave parameters to the present study using Tsallis fits, correlations plots of the fit parameters have been made by considering data at all centralities and collision energies. These plots provide the interdependency of the two fit parameters. This profile plot shows that q and T follow a linear pattern for $\sqrt{s_{NN}} > 27$ GeV. Below this energy, a different pattern is observed, in which, T increases with q from peripheral to mid-central collisions, but above that there is no significant changes in q with an increase in T . This behavior is quite intriguing and has not been observed in case of blast wave fits. Further investigation is needed to understand the full nature of Tsallis fit parameters as a function of collision centrality, collision energy, as well as fitting range of the p_T spectra.

References

1. C. Tsallis, J. Stat. Phys. **52**, 479 (1988).
2. C. Tsallis *et al.*, Physica A **261**, 534 (1998).
3. J. Cleymans and D. Worku, Eur. Phys. J. A **48**, 160 (2012).
4. M. D. Azmi *et al.*, J. Phys. G: Nucl. Part. Phys. **47** 045001 (2020).
5. C. Y. Wong *et al.*, Phys. Rev. D **91** 114027 (2015).
6. H. Zheng and Lilin Zhu, Advances in High Energy Phys. **2015**, 180491 (2015).
7. K. Saraswat *et al.*, J. Phys. Commun. **2** 035003 (2018).
8. R. Si *et al.*, Advances in High Energy Phys. **2018**, 7895967 (2018).
9. K. Shen *et al.*, Eur. Phys. J. A **55** 126 (2019).
10. H. Zhao *et al.*, Advances in High Energy Phys. **2020**, 3724761 (2020).
11. Abhisek Saha and Soma Sanyal, arXiv:2004.03118v1.
12. S. Tripathy *et al.*, Eur. Phys. J. A **52**, 289 (2016).
13. H. Zheng and Lilin Zhu, Advances in High Energy Phys. **2016**, 9632126 (2016).
14. E. Schnedermann, J. Sollfrank and U. W. Heinz, Phys. Rev. C **48**, 2462 (1993).

-
15. L. Adamczyk *et al.*, (STAR Collaboration), Phys. Rev. C **96**, 044904 (2017).
 16. J. Adam *et al.*, (STAR Collaboration), Phys. Rev. C **101**, 024905 (2020).
 17. B. Abelev *et al.*, (STAR Collaboration), Phys. Rev. C **79**, 034909 (2009).
 18. B. Abelev *et al.*, (ALICE Collaboration), Phys. Rev. C **88**, 044910 (2013).
 19. S. Acharya *et al.*, (ALICE Collaboration), Phys. Rev. C **101**, 044907 (2020).
 20. M. D. Azmi and J. Cleymans, Eur. Phys. J. C **75**, 430 (2015).
 21. R. Rath *et al.*, J. Phys. G: Nucl. Part. Phys. **47**, 055111 (2020).
 22. J. Cleymans and D. Worku, J. Phys. G: Nucl. Part. Phys. **39**, 025006 (2012).
 23. C. Y. Wong and G. Wilk, Acta Physica Polonica B, **43**, 2047 (2012).
 24. J. Cleymans *et al.*, Phys. Lett. B **723**, 351 (2013).
 25. M. Rybczynski, Z. Wlodarczyk, Eur. Phys. J. C **74**, 2785 (2014).
 26. M. D. Azmi and J. Cleymans, J. Phys. G **41**, 065001 (2014).
 27. B. I. Abelev *et al.*, (STAR Collaboration), Phys. Rev. C **75**, 064901 (2007).
 28. A. Adare *et al.*, (PHENIX Collaboration), Phys. Rev. C **83**, 052004, (2010).
 29. A. Adare *et al.*, (PHENIX Collaboration), Phys. Rev. C **83**, 064903 (2011).
 30. G. Aad *et al.*, (ATLAS collaboration), New J. Phys. **13**, 053033 (2011).
 31. A. M. Sirunyan *et al.*, (CMS Collaboration) Phys. Rev. D **96**, 112003 (2017).
 32. K. Aamodt, *et al.*, (ALICE Collaboration), Eur. Phys. J. C **71**, 1655 (2011).
 33. B. Abelev *et al.*, (ALICE Collaboration), Phys. Lett. B, **717**, 162 (2012).
 34. S. Acharya *et al.*, (ALICE Collaboration), Eur. Phys. J. C **78**, 263 (2018).
 35. S. Acharya *et al.*, (ALICE Collaboration), Eur. Phys. J. C **80**, 167 (2020).
 36. D. Mishra Ph.D. thesis: "Particle Production Studies in Au+Au and U+U Collisions Using the Detector at RHIC and Understanding the Freeze-out Dynamics".
 37. S. S. Adler *et al.*, (PHENIX Collaboration), Phys. Rev. C **69**, 034909 (2004).
 38. J. Adam *et al.*, (ALICE Collaboration), Phys. Rev. C **93**, 034913 (2016).
 39. B. Abelev *et al.*, (ALICE Collaboration), Phys. Lett. B **720**, 52 (2013).
 40. S. Acharya *et al.*, (ALICE Collaboration), J. High Energy Phys. **11**, 013 (2018).
 41. B. Abelev *et al.*, (STAR Collaboration), Phys. Lett. B **655**, 104 (2007).
 42. B. Abelev *et al.*, (STAR Collaboration), Phys. Rev. Lett. **97**, 152301 (2006).